Two-step hot-pressing sintering of nanocomposite WC–MgO compacts

Jun Ma [a,b], Shigen Zhu [a,b,c,*], Chenxin Ouyang [a,b]

[a] College of Mechanical Engineering, Donghua University, Shanghai 201620, PR China
[b] College of Material Science and Engineering, Donghua University, Shanghai 201620, PR China
[c] Engineering Research Center of Advanced Textile Machinery, Ministry of Education, Shanghai 201620, PR China

Abstract

Two-step hot-pressing sintering (TSS) was applied to consolidate nanocomposite tungsten carbide–magnesia (WC–MgO) powders. The first step sintering was employed at a higher temperature to obtain an initial high density, and the second step was held at a lower temperature by isothermal sintering for several hours to increase bulk density without significant grain growth. The experimental results showed the sintering temperature plays an important role in densification and grain growth of WC–MgO compacts. The optimum TSS regime consisted of heating at 1750 °C (1st step) and 1550 °C (2nd step), resulting in the formation of near full dense microstructure (0.99 TD) with suppressed grain growth (2.59 µm). Accordingly, the improvement on the mechanical properties, including increase in the hardness (from 16.7 to 18.4 GPa), fracture toughness (from 10.2 to 12.95 MPa m$^{1/2}$) and flexural strength (from 976.6 to 1283.7 MPa), was also observed due to the grain refining and full dense bulk.
© 2011 Elsevier Ltd. All rights reserved.

Keywords: Two-step sintering; Nanocomposites; Microstructure-final; Carbides; MgO

1. Introduction

Pure tungsten carbide (WC) powders are usually sintered in the presence of binding materials (typically Co, Fe or Ni) in the liquid phase by various techniques. Metallic binder is introduced to improve WC interparticle binding and to increase the compact toughness. However, metallic binders result in reduced hardness and corrosion/oxidation resistance,[1] and enhance grain growth, particularly in conventional liquid phase sintering due to rapid diffusion in the liquid phase.[2] Therefore, efforts to obtain harder materials have attempted the use of hot-pressing to consolidate WC with low amounts of Co[3] and WC with no metal binder.[4–6]

Among them, a new composite material, WC–MgO is considered as an ideal material for use in industrial applications. Compared with the commercial micron- and submicron-grained structure WC–Co composites, the WC–MgO can achieve superior high value of hardness and toughness combination.[7] Researches[8–11] have been focused on the synthesis of the pow-ders, but fewer on its consolidation details. We have recently attempted to prepare this MgO particulate toughened WC matrix composite using hot-pressing sintering method. It has been found that the sintering activity and densification response of the hot-pressing processed WC–MgO were not as good as those consolidated *via* spark plasma activated sintering (PAS). The PAS method has yielded such benefits as a rapid sintering rate, high densification, and fine grain size production. Nevertheless, PAS method is hardly accessible and scarcely used for practical applications.

Fortunately, the experimental results revealed that the afore-mentioned problems can be well-resolved by adding the rare earth (RE) oxide in the elemental powder system. In our previous works, La$_2$O$_3$ was selected as the addition to WC–MgO during its bulk synthesis process. The results indicated that the La$_2$O$_3$-WC/MgO compact can achieve the high relative density and homogenous microstructure consisting of small grains.[12] However, the effectiveness of the additives greatly depends on the homogeneity of their distribution. While excess La$_2$O$_3$ was added to WC–MgO, these particles located at grain boundaries may result in the increasing of the grain boundary width. It may cause technique problems for the fabrication of uniform, dense and ultrafine structure.

* Corresponding author at: College of Mechanical Engineering, Donghua University, Shanghai 201620, PR China. Tel.: +86 21 6779 2813; fax: +86 21 6779 2813.
E-mail address: sgzhu@dhu.edu.cn (S.G. Zhu).

Another way to control the grain growth during consolidation is to use novel processing technique to tailor the microstructure. In recent years, a two-step sintering (TSS) method has been proposed to achieve the densification of ceramic bodies without significant grain growth in the final stage of sintering.[13] The TSS procedure consists of the following steps: (1) reaching a high temperature (T_1) to conduct first-step sintering until the relative sample density > 75% theoretical density (TD) is achieved; (2) lowing the temperature to T_2 to conduct second-step sintering during which there is only densification and no grain growth.[13,14] So far, the TSS method has been successfully applied to the sintering of Y_2O_3,[13,15] Ni–Cu–Zn ferrite,[16] $BaTiO_3$,[17–19] Al_2O_3[20,21] and liquid-phase sintering of SiC[22] as well as doped ZnO varistors.[23]

According to the reported works, achieving a high density and a small grain size is very important for the structural ceramic materials because it can bring about an improvement of mechanical properties such as hardness, wear resistance, strength or fracture toughness.[24] In this work, two-step sintering is applied on the preparation of high-density WC-4.3 wt% MgO compact with refined grains. Preliminary investigation on the bulk density and microstructural evolution during constant-heating-rate and isothermal sintering are carried out in order to determine the appropriate heating temperatures T_1 and T_2. Thereafter, the suggesting temperatures T_1 and T_2 are practiced in the present work, and the effects of the applied TSS process on the structural properties of WC–MgO are discussed. A comparison is also made of the mechanical properties of the compacts made by TSS technique with those of the normally hot-pressing sintered ones.

2. Experimental

Experiments consisted of synthesis, characterization, sintering and mechanical properties determination of WC–MgO samples according to the following methods.

2.1. Powder synthesis and characterization

Nanocrystalline WC-4.3 wt% MgO was synthesized *via* mechanical alloying process in a QM-1SP4 high energy planetary ball mill machine. The starting materials were WC (75 μm, 99.5% purity) and MgO (48 μm, 98.5% purity). The ball mill process was carried out under argon gas atmosphere at a rotational speed of 350 revolutions per minute (rpm) for 50 h. The ball-to-powder weight ratio was 10:1. The milling balls (10 mm in diameter) and vial were made of cemented carbide materials.

The morphologies of the as-milled powders were investigated by transmission electron microscope (TEM) on a JEOL JEM-2100F electron microscope. The phases identification were observed by X-ray diffraction (XRD) on a D/max-2550 PC (Rigaku Co., Japan) X-ray diffractmeter with a Cu K_α radiation ($\lambda = 0.154$ nm) at 40 kV and 300 mA. The specific surface area of the powders was determined using Brunauer–Emmett–Teller (BET) surface area analyzer (Autosorb-1, Quantachrome, United States). The particle size of the powders was measured

by dynamic laser light scattering method (DLLS, BI-200SM, Brookhaven, United States).

2.2. Conventional hot-pressing sintering and two-step hot-pressing sintering

Sintering of the samples was implemented by conventional hot-pressing sintering (CS) and two-step hot-pressing sintering (TSS). The as-milled composite powders were hot-pressed in a graphite die at 1450–1900 °C in a vacuum of 1.3×10^{-1} Pa with 50 °C temperature intervals and a heating ramp of 10 °C/min. The specimens were held at the highest temperature for 3 min with the pressure of 39.6 MPa in order to obtain a uniform temperature throughout the sample. The consolidated bulks with a dimension of $\varnothing$ 15 × 15 mm^3 were obtained for the properties tests. For the first step of TSS, samples were heated under the same conditions as conventional sintering. The cooling rate of TSS between T_1 and T_2 was 60 °C/min. The samples were held at T_2 up to 8 h with the pressure of 39.6 MPa so as to reach a higher density.

The densities of the sintered bulks were determined by Archimedes' principle, using deionized water immersion, with an analytical balance. Comparing this value with that calculated from the role of mixture principle, the relative density of the compacted bulks was achieved. The samples were ground and polished by standard ceramographic methods and then etched in a Murakami's reagent consisting of $Fe_3[K(CN)_6]$ (10 g), KOH (10 g) and distilled water (100 ml) for 5 min to expose the grain boundaries. The microstructure of the bulks was observed by scanning electron microscope (SEM, S-4800, Hitachi Co., Japan) of the polished and etched surface. The grain size was estimated by the linear intercept method. For each sample, at least three images were taken of the microstructure; in each image a minimum of five line segments were assessed. The particulate/matrix interfacial microstructures were characterized by scanning probe microscope (SPM, NanoScope IV, United States).

2.3. Mechanical properties

The hardness was determined using a HVS-50Z Vickers indenter with a load of 30 kg and an indentation time of 10 s. The resulting indentation cracks were used as an indication of the fracture toughness (K_c) of the sample.[25] We should note that the Vickers hardness measurements that were made a rough approximation for the valid K_c test. Hence, they were an approximation of the expected fracture–toughness measurements, not an absolute determination. At least ten indentations were made and the average value was obtained. Flexural strength of sintered samples was measured using three-point flexure test according to the ASTM B312 standard. Sample bars were cut from the sintered pellets and then ground and polished into 15 mm × 5 mm × 3 mm specimens. Three-point flexure tests were carried out at room temperature with a span of 12 mm and cross-head speed of 0.01 mm/s. The fracture strength of consolidated samples (the average of five tests) was calculated
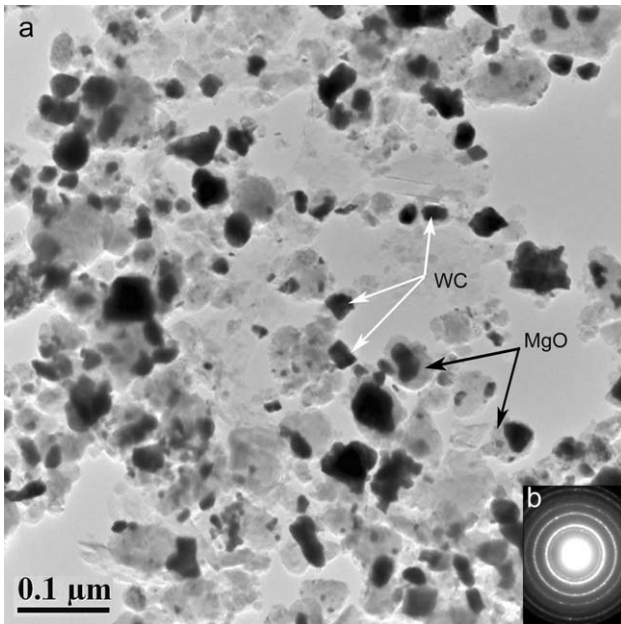
Fig. 1. Transmission electron micrograph and selected area diffraction pattern (SADP) of nanocomposite WC–MgO powders after 50 h of the ball-milling time.

using

$$\sigma = \frac{3PL}{2t^2 w} \qquad (1)$$

where σ (MPa) is flexural fracture strength, $P(N)$ is the force required to rupture, L ($L = 12$ mm) is the length of the span of fixture, w ($w = 5$ mm) is the width of the specimen, and t ($t = 3$ mm) is the thickness of specimen.

3. Results and discussion

3.1. Powder characterization

Fig. 1 shows the morphology of the as-milled WC–MgO composite powder. It can be observed that the particles have a size range of 10–50 nm and a mainly irregular polygonal shape. The average particle size of the nanocomposite powder (35 nm) was determined by dynamic laser light scattering (DLLS) method. Results of BET test were used to decide the effect of milling on the surface area of the powders. The data revealed a nearly 60.3% increase in the surface area of the powder from 11.6 to 18.6 m^2 g^{-1} during milling. The diffractogram shown in Fig. 2 presents the XRD pattern of the WC–MgO composite powders. After milling for 50 h, the diffraction peaks corresponding to WC and MgO phases were mainly detected. But amounts of W$_2$C phases were seen in the as-milled powders as well, which might be due to the carbon deficient during ball mill process. The average crystallite size of the powder was calculated by means of the X-ray line-broadening method[26] to be 34.7 nm, from which the grain size and microstrain were obtained. The crystallite size was in good agreement with the TEM observation and DLLS measurement.
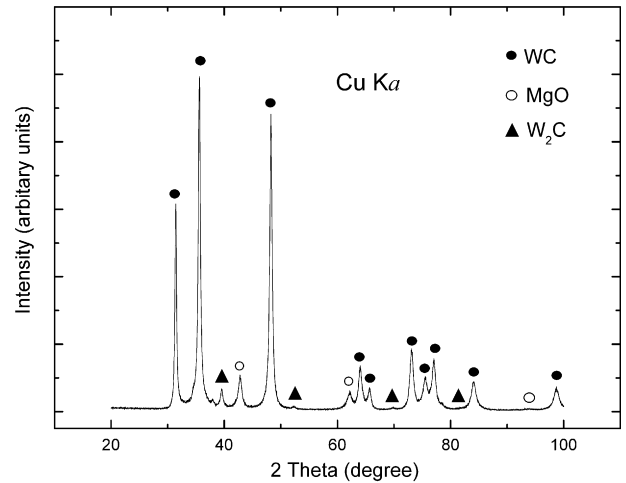

Fig. 2. X-ray diffraction pattern of nanocomposite WC–MgO powders.

3.2. Criterion for determining sintering temperature

Fig. 3 shows the effect of sintering temperature on densification and grain size of the specimens made of nanocomposite WC–MgO after conventional hot-pressed sintering (CS). The density versus temperature plot illustrated a sigmoidal shape in the temperature range of 1450–1900 °C. No significant densification was observed below 1650 °C. The rate of densification increased dramatically at ∼1700 °C and a significant densification was obtained at about 1750 °C. It is seen that the increase of temperature from 1450 to 1750 °C results in the relative density changing from 0.79 to 0.93 of theoretical density (TD). Further increase in temperature (from 1750 to 1850 °C) results in a slighted density enhancement of up to 6%.

The change of grain size as a function of sintering temperature shows two distinct regions. At first region, starting at 1450 °C and continuing up to 1750 °C, the average grain size of the bulks does not tend to show a dramatic change. According to the solid
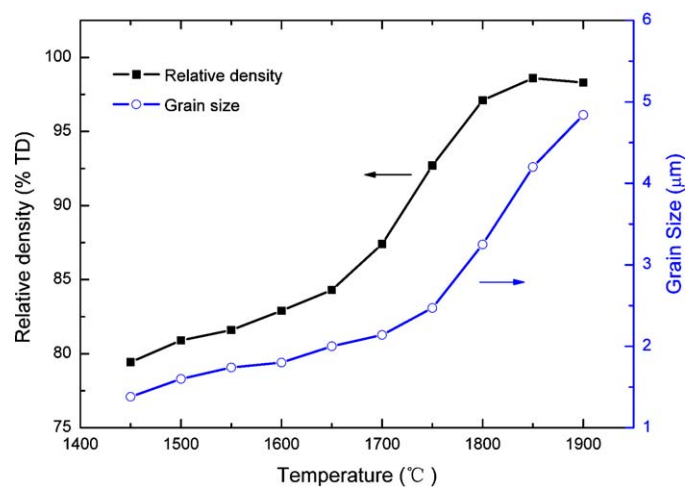

Fig. 3. Relative density and grain size of the nanocomposite WC–MgO compacts as a function of sintering temperature under conventional hot-pressing sintering (CS) condition with the holding time for 3 min to obtain a uniform temperature throughout the sample.
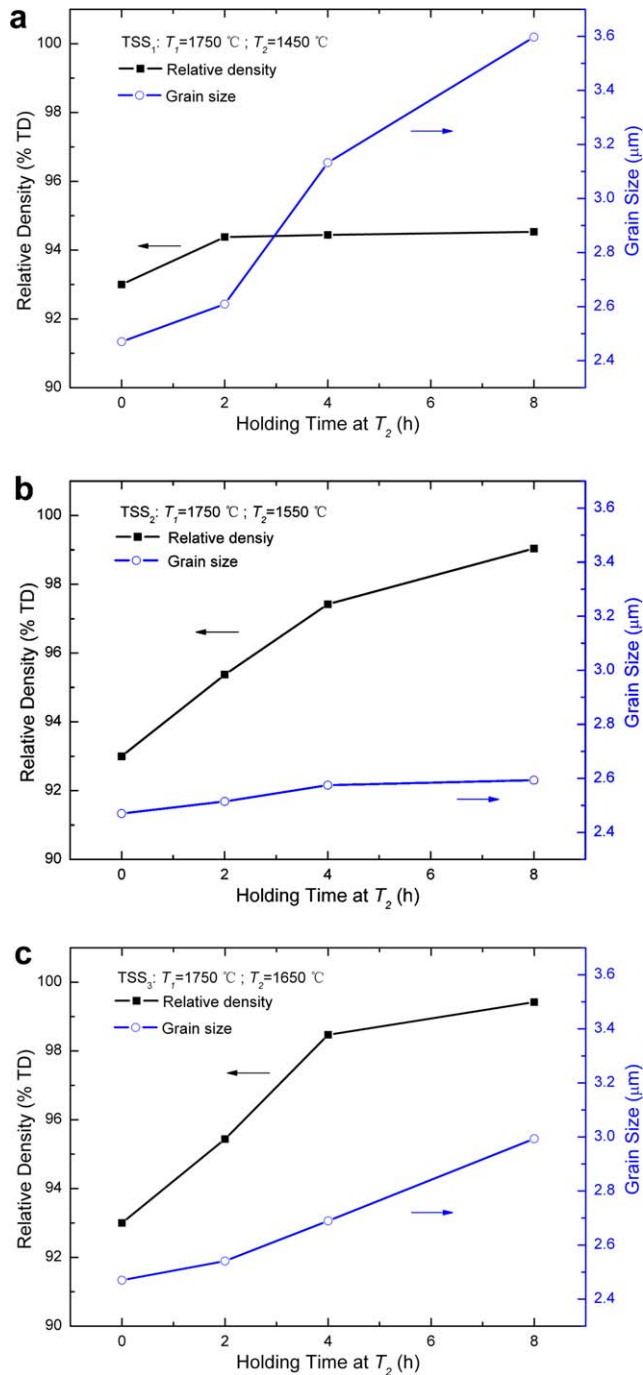
Fig. 4. Relative density and grain size of the WC–MgO compacted bulks versus various holding time under (a) TSS$_1$ conditions ($T_1 = 1750\,°C$, $T_2 = 1450\,°C$), (b) TSS$_2$ conditions ($T_1 = 1750\,°C$, $T_2 = 1550\,°C$) and (c) TSS$_3$ conditions ($T_1 = 1750\,°C$, $T_2 = 1650\,°C$).

Fig. 5. Scanning electron micrograph of WC–MgO compacts prepared under (a) CS conditions (1850 °C/0 h), (b) CS conditions (1550 °C/8 h) and (c) TSS$_2$ conditions ($T_1 = 1750\,°C$, $T_2 = 1550\,°C$/8 h).

state sintering mechanism,[15] when the relative density is usually between 0.65 and 0.90 TD, dispersed open pores could pin grain boundaries and hinder grain boundary migration, for which the grain growth was suppressed. In contrast, as shown in Fig. 3, a very sharp ascending of grain size from 2.5 to 4.8 μm can be observed when the temperature increased from 1750 to 1900 °C. It shows a considerable grain growth in the final stage of sintering taking place at 1900 °C. Yet, the density does not show
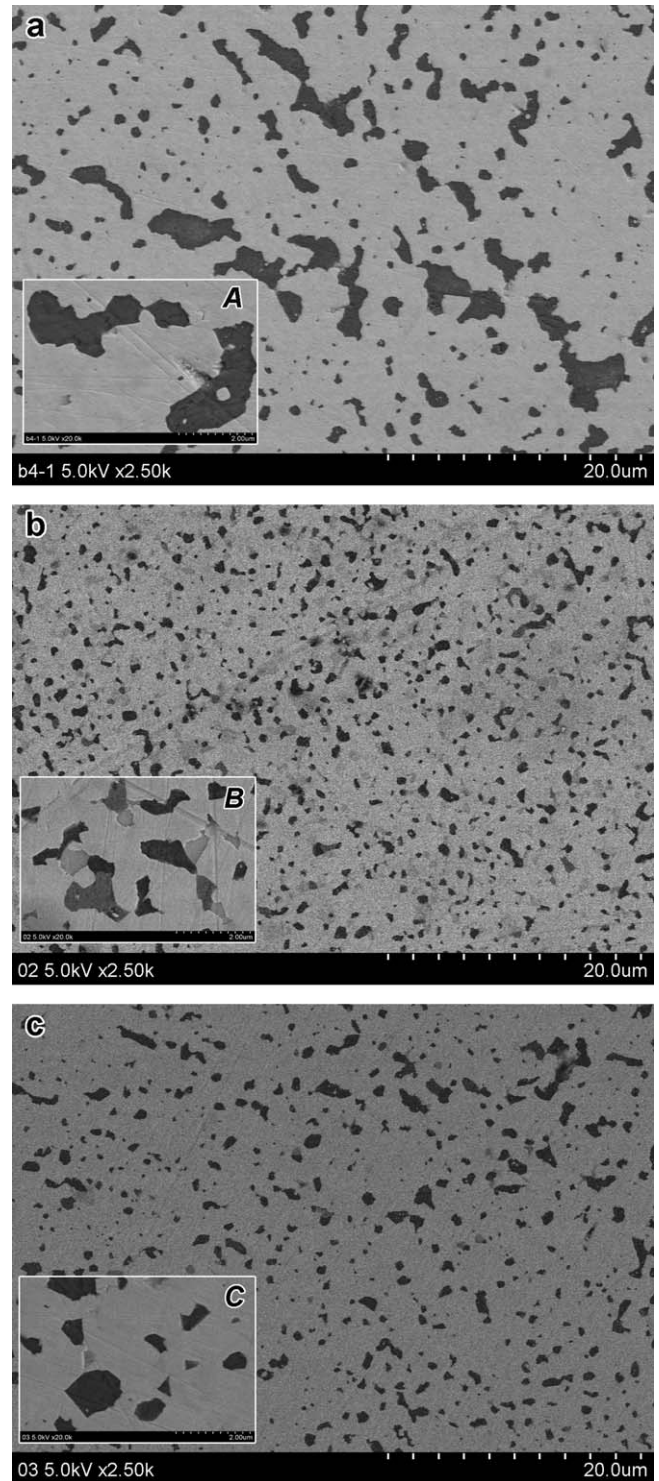
a remarkable increase (from 0.93 to 0.98 TD). It has been confirmed that the open pores (referring to the intermediate stage of sintering) collapsed to form closed ones after the final stage started. Such a collapse results in a substantial decrease in pore pinning, which triggers the accelerated grain growth.[27–29]
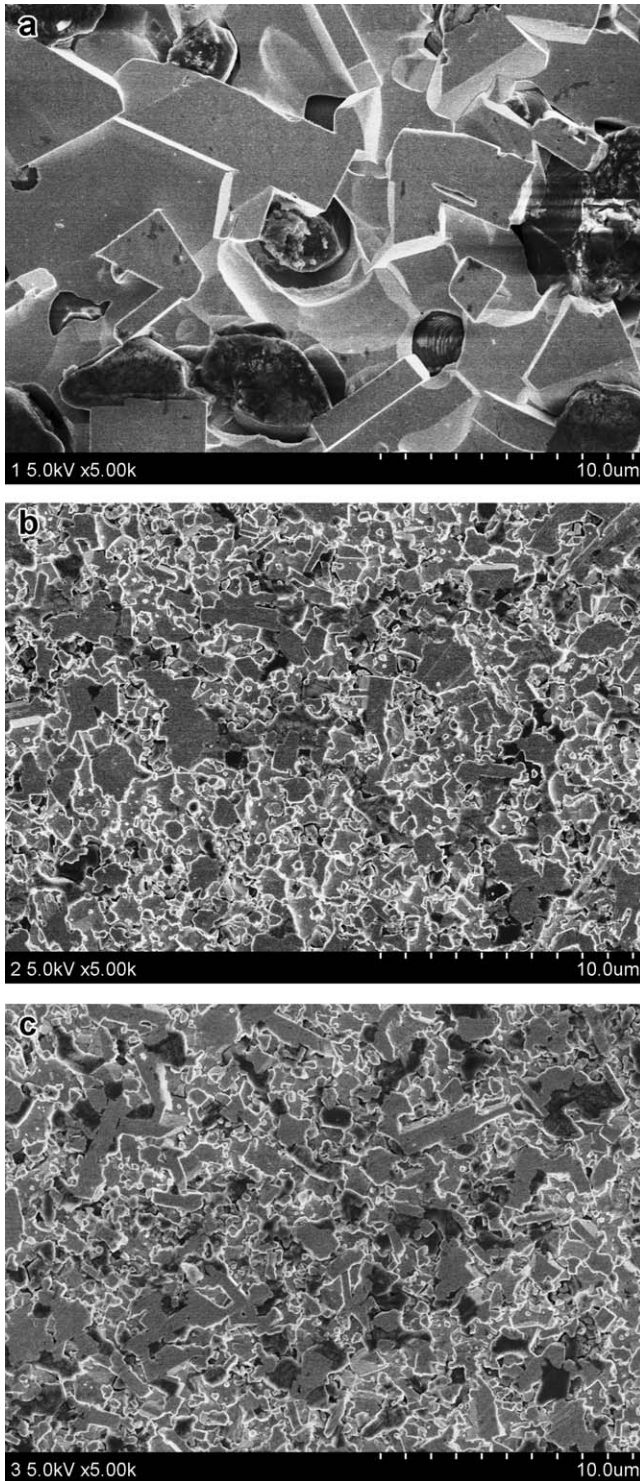
Fig. 6. SEM images of the etched samples showing the different microstructures of the matrixes consolidated under (a) CS conditions (1850 °C/0 h), (b) CS conditions (1550 °C/8 h) and (c) TSS$_2$ conditions (T_1 = 1750 °C, T_2 = 1550 °C/8 h).

Table 1
Conditions for two-step sintering regimes.

Regimes	T_1 (°C)	T_2 (°C)	Holding time at T_2 (h)
TSS$_1$	1750	1450	2-4-8
TSS$_2$		1550	2-4-8
TSS$_3$		1650	2-4-8

which all pores in the sample are unstable and shrinkable, and the grain growth may be triggered. The temperature of the first step (T_1) was chosen on the basis of CS result. The result reveals that the relative density increases with the temperature to a significant enhancement in the range of 1700–1800 °C. A noticeable grain growth is observed when the temperature is higher than 1750 °C (Fig. 3). It is known that the grain growth increases the diffusion distance and makes the sintering become more difficult.[30] The state of the compacts after the first step sintering critically influences the subsequent step, and the grain growth caused by over-heating must be cautiously avoided. Accordingly, the first step temperature (T_1) is set at 1750 °C where the densification shows a big slope in the course of conventional sintering, and the corresponding relative density is from 0.79 to 0.93 TD.

Considering the determination of temperature T_2 for the second step sintering, Mazaheri et al.[31] reported that there is a critical temperature for the second step to obtain fully dense structure without accelerated grain growth. At temperatures lower than that, even after long term isothermal holding, no improvement in densification can be achieved, *i.e.* two-step sintering carried out at second step temperature (T_2) lower than the critical one turned out to be a disappointing process; in contrary the grain growth may generated when the setting T_2 is too high. In this work, T_2 was set in the range of 1450–1650 °C, since temperature in this range was associated with a relatively slow rate of grain growth according to the previous CS experiment.

3.3. Microstructure evolution in two-step sintering

Table 1 lists the conditions under which TSS regimes were carried out. Under TSS$_1$ sintering regime, T_1 and T_2 were 1750 °C and 1450 °C. The relative density of the sample at the end of first step was 0.93 TD, which was obtained from the CS result at 1750 °C (Fig. 3). The changes in the relative density and grain size with the holding time obtained from TSS$_1$ regime are shown in Fig. 4a. A slight density increase of 0.01 TD (from 0.93 to 0.94 TD) can be observed while there is an obvious average grain size increase of 1.13 μm during this time span. A similar trend has also been reported for the TSS behavior of ZnO[31] and Y$_2$O$_3$.[32] It has been confirmed that the reason for exhaustion of densification in the second step is attributed to the low temperature (T_2) which retards grain-boundary diffusion (GBD) as the sintering mechanism,[15] but the surface diffusion remains active.

When conventional hot-pressing sintering was carried out at 1450 °C, the relative density was 0.81 TD with little improvement even though the holding time was increased to 4 h and a finger-like growth among WC particles occurred, indicating that the sintering mechanism *via* surface diffusion was

On the purpose of suppressing the grain growth at final sintering stage, two-stage sintering (TSS) technique was applied. According to the previous researches,[13,15] the success of TSS greatly relies on the selecting of temperatures T_1 and T_2. Usually, a sample is sintered to a higher temperature T_1 to yield a relative density between 0.75 and 0.92 TD, corresponding to a state in

performed at 1450 °C through the diffusions of atoms along the surface of nearby particles.[33] In other words, densification occurred only when the distances between the centers of the crystallites was diminished. The decreases in distance need an off-transport of matter from grain boundaries to the neck. Therefore, the densification was hard to be achieved without volume and grain-boundary diffusion. Meanwhile, the surface diffusion only contributes to neck growth and grain growth without any improvement on densification. As a result, the low temperature of the second step in TSS_1 not only fails to achieve the densified structure but results in a grain growth as well.

By contrast, under TSS_2 regime ($T_1 = 1750$ °C and $T_2 = 1550$ °C) nearly full dense structure was obtained although T_1 is the same for both TSS_1 and TSS_2 regimes. Fig. 4b illustrates the densities and grain sizes of TSS_2 samples against the holding time. No significant increase in the grain size but a remarkable densification occurred, when the sample was held at T_2 (1550 °C). According to Fig. 4b, while the relative density increases to 0.99 TD, the average grain size slight increases from 2.47 to 2.59 μm ($t = 8$ h). Compared with Fig. 4a, it can be observed that in the second step of TSS_2, densification proceeds with a rather constant grain size. Chen and Wang[13,15,16,32] have explained that to achieve densification without grain growth, grain-boundary diffusion should remain active while the grain boundary migration is to be suppressed. The grain growth entails a competition between grain-boundary mobility and junction mobility. Once the latter becomes less at relatively lower temperatures in which junctions are rather motionless, the mentioned drag would occur. A mechanism to inhibit grain-boundary movement is a triple-point (junction) drag, and it is essential to decrease grain-boundary mobility to prevent accelerated grain growth.[15] Consequently, similar results were obtained from the present work. The grain-boundary diffusion, accompanied by triple-point drag at relatively lower temperatures ($T_2 = 1550$ °C), contributes to a full dense microstructure with a constant grain size.[13]

Moreover, the increase on the initial density after the first step guarantees the success of the TSS procedure as well. When isothermal sintering was performed at 1550 °C, the relative density increased from 0.82 to 0.92 TD with the holding time prolonged to 8 h. Fig. 6b shows the SEM micrograph of the etched sample sintered under CS regime (1550 °C/8 h). In comparison with the results obtained under TSS_2 regimes (Fig. 6c), the average grain size of both samples was 2.59 μm and little difference on the average grain size can be observed, while the relative density of the TSS_2 sintered bodies achieved 0.99 TD. It has been discussed previously that a higher temperature T_1 occurs at 1750 °C which is advantageous for the densification. When a sufficiently high starting density was obtained during the first step, the pores become subcritical and unstable and can be filled as long as grain boundary diffusion allows.[34] Hence, the high temperature T_1 in the first step was essential for achieving a successful TSS regime.

Fig. 4c plots the variation of relative density and grain size versus holding time at $T_2 = 1650$ °C for the samples firstly heated up to 1750 °C (TSS_3). Although the temperature T_2 was increased 100 °C in the second step, structure with an average

grain size of 2.99 μm was obtained, *i.e.* the increase on grain growth was observed. The grain size can be controlled below 3 μm, but the grain size curve exhibits an oblique slope tendency. Fig. 4 indicates the importance of the second step sintering temperature. The low temperature isothermal sintering in the second step might fail to eliminate the residual porosity. Meanwhile, the high temperature soaking might lead to a grain growth. Accordingly, a critical temperature ($T_2 = 1550$ °C) between 1450 and 1650 °C was chosen as the second step sintering temperature for eliminating the residual porosity and achieving near full dense structure without accelerated grain growth.

Fig. 5 shows the SEM pictures of the fully dense WC–MgO compacts after sintering under conventional and two-step hot-pressing sintering process. The sample obtained from CS was sintered at 1850 °C and at 1550 °C for 8 h, whereas those obtained from TSS were processed under TSS_2 regime (the holding time at T_2 was 8 h). The EDS spot analysis reveals that the grey-dark particulates were composed of the Mg and O elements, while the surrounding grey matrix was rich in the W and C elements. It can be concluded that the MgO particulate toughened WC matrix composites can generally be prepared. However, the dispersion states of the MgO particulates were significantly influenced by the sintering temperature, which might be the reason why the volume fraction of MgO phase looks different in Figs. 5a–c. Under CS regime (1850 °C), the MgO particulates showed an irregular polygonal shape and were larger than 2.5 μm in size (Fig. 5a-A), *i.e.* the aggregation of magnesia particulates was occurred due to the high sintering temperature. Compared with that, the toughening particulates in the compact sintered under lower temperature CS regime (1550 °C/8 h, Fig. 5b) and TSS_2 (Fig. 5c) were presented in a refine and dispersed morphology.

The characteristic microstructures of the etched samples are shown in Fig. 6. A number of SEM photos similar to that of Fig. 6 were used to evaluate the grain size of the sintered bulks. When the bulk sintered under CS regime (1850 °C), significantly coarsened WC grains were formed (Fig. 6a). Under TSS_2 regime, the refined grains were visible and the toughening particulates were dispersed uniformly in such grains (Fig. 6c). Therefore, the grain growth was prohibited under TSS_2 condition. This indicates that TSS_2 is capable of producing a fully dense microstructure accompanied by a suppressed grain growth.

Fig. 7 shows the particulates/matrix interfacial microstructures in the compacts which were sintered under CS (1850 °C) and TSS_2 conditions. The test samples were polished with diamond paste to 0.05 μm surface finish, the polished surface was also cleaned with acetone for the characterization. In the samples consolidated by CS method (1850 °C), the toughening particulates showed a fluctuated and rough morphology (Fig. 7a). It is reasonable to consider that the MgO particulates were separated incompletely. Interestingly, under the TSS_2 sintering regime, the MgO particulates were presented in a smoothened and dispersed appearance (Fig. 7b). As to the particulates/matrix interfacial characteristics in this instance, it revealed that the toughening particulates in the compact sintered under TSS_2 con-
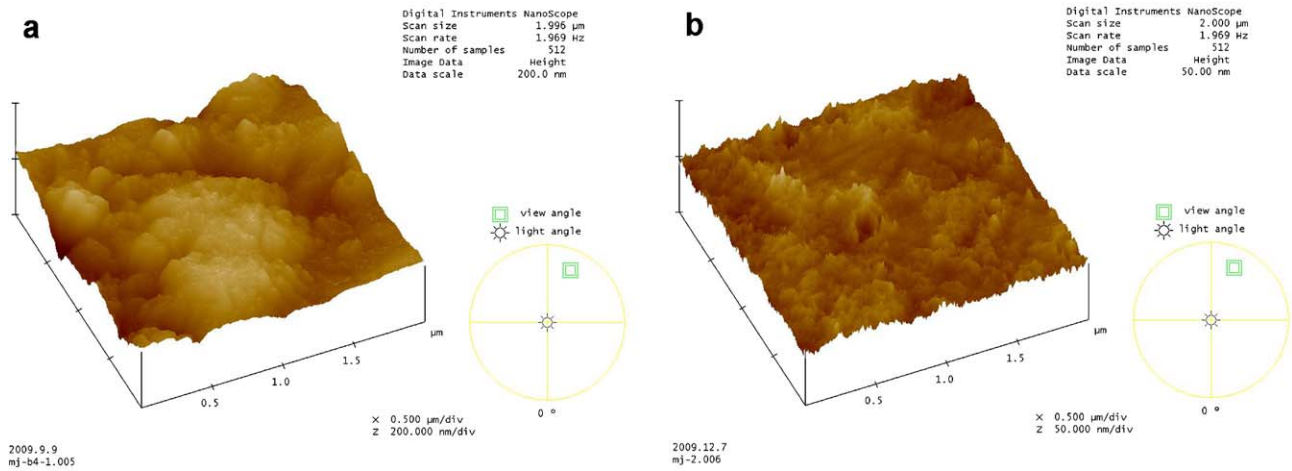
Fig. 7. 3D SPM images showing the particulates/matrix interfacial microstructures in the compacts consolidated under (a) CS conditions (1850 °C/0 h), (b) TSS$_2$ conditions ($T_1 = 1750$ °C, $T_2 = 1550$ °C/8 h).

ditions had the continuous and compatible interfaces with the matrix.

3.4. Mechanical properties of the bulks

In Table 2, we provide a comparison of the mechanical properties of the compact obtained under the CS (1850 °C) and TSS$_2$ regimes. The maximum relative density of both samples was above 0.98 TD. The hardness and fracture toughness were measured on the polished sections. It is clear that under CS regime, the hardness was about 16.7 GPa and estimated fracture toughness was 10.2 MPa m$^{1/2}$. This can be attributed to the coarse matrix grains and the MgO agglomeration segregation throughout the sintered structure. It is well known that in order to achieve better mechanical strength and improve toughness of ceramics, one could use grain refining mechanism.[24] In the present study, without the addition of any dopant, the grain size of the matrix was decreased from 4.2 μm to 2.59 μm due to the two-step sintering process without any deterioration of the densification. Consequently, the hardness increased from 16.7 to 18.4 GPa

and was probably affected by the grain refinement in the matrix.

Indent cracks were made on the polished surface of composite after hardness test to clarify further the toughening effect that is responsible for rising toughness behavior. The crack growth path corresponding with the extended radial cracks of 30 kg Vickers indentation on the surface of WC–MgO composite sintered by TSS$_2$ is shown in Fig. 8. Extensive crack interactions, i.e. mainly crack bridging were observed (Fig. 8a), indicating that once the crack has reached the particle–matrix interface, the difference in the crack-tip opening displacement between the ductile particle and the brittle matrix will cause crack to be locally blunted, thus produce closure stress bridging the crack along its length.[35] These effects require more external load to force the crack propagate further, thus induce improvement of toughness. In addition, crack deflections that enhance the energy for crack growth were also observed (Fig. 8b). As a result, the fracture toughness varied between 10.2 and 12.95 MPa m$^{1/2}$. This was influenced by the well-dispersed toughening particulates and the same features which affected the hardness. Correspondingly, the flexural
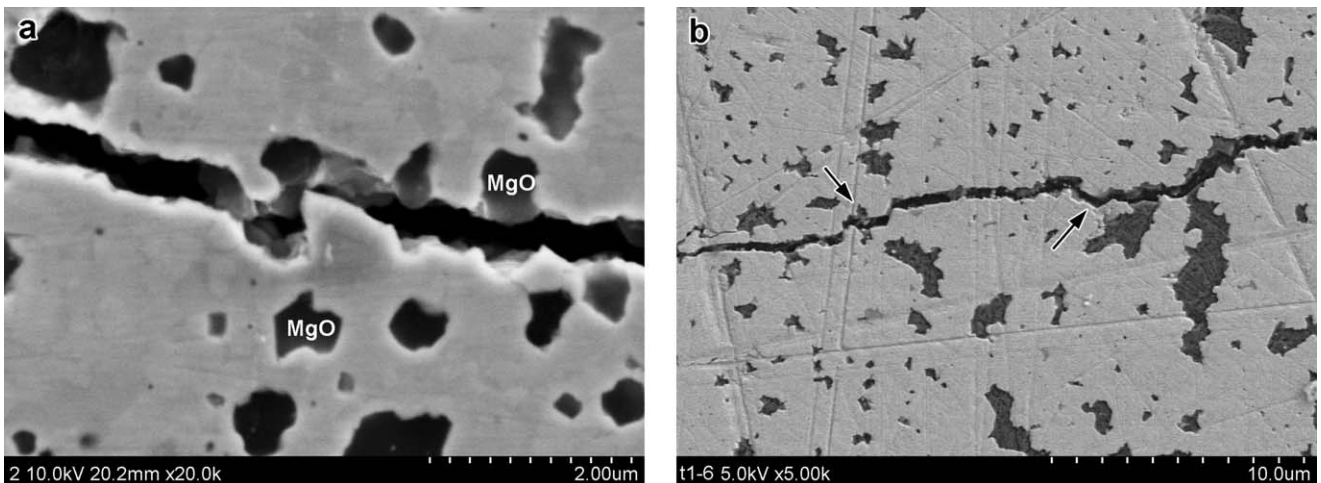

Fig. 8. (a) Indent crack bridging and (b) deflection of WC–MgO composite.

Table 2
Mechanical properties of nanocomposite WC–MgO compacts sintered by CS (1850 °C) and TSS$_2$ regimes.

Sintering method	Relative density (% TD)	Vickers hardness (HV/GPa)	Fracture toughness (K_c/MPa m$^{1/2}$)	Flexural strength (σ/MPa)
CS (1850 °C)	98.6	16.7 ± 0.6	10.2 ± 0.9	976.6 ± 85.9
TSS$_2$	99	18.4 ± 0.5	12.95 ± 0.5	1283.7 ± 126.6

strength of TSS$_2$ sample (1283.7 MPa) was higher than that consolidated by conventional sintering (976.6 MPa), and was very close to the WC-3–8 wt% Co hard alloy (1150–1650 MPa).[36]

4. Conclusions

Nanocomposite WC–MgO powders were synthesized using high-energy planetary ball milling method. Based on the experimental results, the following conclusions can be obtained regarding the feasibility of the two-step hot-pressing sintering for WC-4.3 wt% MgO powders:

(1) Two-step sintering conducted at $T_1 = 1750$ °C and $T_2 = 1550$ °C leads to a fully dense structure, accompanied a magnificent suppression of grain growth. Temperature T_1 for the first step sintering was selected from the densification rate during conventional hot-pressing sintering. For the choice of T_2, the surface diffusion has to be considered. At a relatively lower second step temperature (*i.e.* TSS$_1$ under $T_2 = 1450$ °C), no densification but a remarkable grain growth was observed even after a prolonged isothermal treatment.

(2) A high relative density over 0.99 TD with refine grain size (2.59 μm) is achieved after applying the two-step hot-pressing sintering process (TSS$_2$). A comparison with the conventional hot-pressing sintering (CS) shows that the grain size was decreased from 4.2 μm (for CS under $T = 1850$ °C) to 2.59 μm (for TSS$_2$ under $T_2 = 1550$ °C).

(3) Microstructure of the TSS$_2$ sample was finer and more homogenous than the sample consolidated under CS conditions, leading to a higher hardness value of about 18.4 GPa compared to 16.7 GPa obtained for CS sample. Three-point flexural strength of TSS$_2$ (1283.7 MPa) was higher than that (976.6 MPa) for CS sample. The estimated fracture toughness was also increased from 10.2 MPa m$^{1/2}$ (for CS sample) to 12.95 MPa m$^{1/2}$ (for TSS$_2$ sample). The improved mechanical properties of WC–MgO composite prepared by TSS$_2$ method are attributed to the grain refinement, well dispersed toughening particulates and the crack bridging effect.

Acknowledgement

References

1. Kim HC, Shon IJ, Garay JE, Munir ZA. Consolidation and properties of binderless sub-micron tungsten carbide by field-activated sintering. *Int J Refract Met Hazard Mater* 2004;**22**:257–64.
2. Kim HC, Shon IJ, Yoon JK, Doh JM. Consolidation of ultra fine WC and WC–Co hard materials by pulsed current activated sintering and its mechanical properties. *Int J Refract Met Hazard Mater* 2007;**25**: 46–52.
3. Li T, Li QF, Fuh JYH, Yu PC, Wu CC. Effects of lower cobalt binder concentrations in sintering of tungsten carbide. *Mater Sci Eng A* 2006;**430**:113–9.
4. Sugiyama S, Taimatsu H. Preparation of WC–WB–W$_2$B composites from B$_4$C–W–WC powders and their mechanical properties. *Mater Trans* 2002;**43**:1197–201.
5. Cha SI, Hong SH. Microstructures of binderless tungsten carbides sintered by spark plasma sintering process. *Mater Sci Eng A* 2003;**356**: 381–9.
6. Sugiyama S, Taimatsu H. Mechanical properties of WC–WB–W$_2$B composites prepared by reaction sintering of B4C–W–WC powders. *J Eur Ceram Soc* 2004;**24**:871–6.
7. El-Eskandarany MS. Fabrication of nanocrystalline WC and nanocomposite WC–MgO refractory materials at room temperature. *J Alloys Compd* 2000;**296**:175–82.
8. Wu CX, Zhu SG, Ma J, Zhang ML. Synthesis and formation mechanisms of nanocomposite WC–MgO powders by high-energy reactive milling. *J Alloys Compd* 2009;**478**:615–9.
9. Ma J, Zhu SG, Wu CX, Zhang ML. Application of back-propagation neural network technique to high-energy planetary ball milling process for synthesizing nanocomposite WC–MgO powders. *Mater Des* 2009;**30**:2867–74.
10. Zhang ML, Zhu SG, Ma J, Wu CX, Zhu SX. Synthesis of nanosized WC/MgO powders by high energy ball milling and analysis of reaction thermodynamics. *Powder Metall* 2010;**53**:169–73.
11. Zhang ML, Zhu SG, Ma J, Wu CX. Preparation of WC/MgO composite nanopowders by high-energy reactive ball milling and their plasma-activated sintering. *Powder Metall Met Ceram* 2008;**47**, 525 230.
12. Ma J, Zhu SG, Di P, Zhang Y. Influence of La$_2$O$_3$ addition on hardness, flexural strength and microstructure of hot-pressing sintered WC–MgO bulk composites. *Mater Des* 2011;**32**:2125–9.
13. Chen IW, Wang XH. Sintering dense nanocrystalline oxide with-out final stage grain growth. *Nature* 2000;**404**:168–71.
14. Maca K, Pouchly V, Zalud P. Two-step sintering of oxide ceramics with various crystal structures. *J Eur Ceram Soc* 2010;**30**:583–9.
15. Wang XH, Chen PL, Chen I. Two-step sintering of ceramics with constant grain size, I. Y$_2$O$_3$. *J Am Ceram Soc* 2006;**89**:431–7.
16. Wang XH, Deng XY, Bai HL, Zhou H, Qu WG, Li LT, Chen IW. Two-step sintering of ceramics with constant grain-size, II: BaTiO$_3$ and Ni–Cu–Zn ferrite. *J Am Ceram Soc* 2006;**89**:438–43.
17. Polotai A, Breece K, Dickey E, Randall C. A novel approach to sintering nanocrystalline barium titanate ceramics. *J Am Ceram Soc* 2005;**88**:3008–12.
18. Karaki T, Yan K, Adachi M. Barium titanate piezoelectric ceramics manufactured by two-step sintering. *Jpn J Appl Phys* 2007;**46**:7035–8.
19. Wang DH, Deng XY, Bai HL, Zhou H, Qu WG, Li LT. Two-step sintering of ceramics with constant grain size, II: BaTiO$_3$ and Ni–Cu–Zn ferrite. *J Am Ceram Soc* 2006;**89**:438–43.
20. Li J, Ye Y. Densification and grain growth of Al$_2$O$_3$ nanoceramics during pressureless sintering. *J Am Ceram Soc* 2006;**89**:139–43.
21. Bodisova K, Sagalik P, Galusek D, Svancarek P. Two-stage sintering of alumina with submicrometer grain size. *J Am Ceram Soc* 2007;**90**:330–2.

22. Lee YI, Kim YW, Mitomo M, Kim DY. Fabrication of dense nanostructured silicon carbide ceramics through two-step sintering. *J Am Ceram Soc* 2003;**86**:1803–5.

23. Duran P, Tartaj J, Moure C. Fully dense, fine-grained, doped zinc oxide varistors with improved nonlinear properties by thermal processing optimization,. *J Am Ceram Soc* 2003;**86**:1326–9.

24. Krell A, Blank P. The influence of shaping method on the grain size dependence of strength in dense submicrometer alumina. *J Eur Ceram Soc* 1996;**16**:1189–200.

25. Shetty DK, Wright IG, Mincer PN, Clauer AH. Indentation fracture of WC–Co cermets. *J Mater Sci* 1985;**20**:1873–82.

26. Ramarao P, Anantharaman TR. X-ray line breadth analysis of deformed metals. *Z Metallkd* 1963;**54**:658–63.

27. Duran P, Capel F, Tartaj J, Moure C. Sintering behavior and electrical properties of nanosized doped-ZnO powders produced by metallorganic polymeric processing. *J Am Ceram Soc* 2001;**84**:1661–8.

28. Kang SJL. Sintering densification. In: *Grain Growth and Microstructure.* Oxford: Elsevier; 2005.

29. Rahaman MN. *Ceramic Processing and Sintering*. 2nd edition New York: Marcel Dekker Inc.; 2003.

30. Mazaheri M, Valefei M, Razavi Hesabi Z, Sadrnezhaad SK. Two-step sintering of nanocrystalline $8Y_2O_3$ stabilized ZrO_2 synthesized by glycine nitrate process. *Ceram Int* 2009;**35**:13–20.

31. Mazaheri M, Zahedi AM, Sadrnezhaad SK. Two-step sintering of nanocrystalline ZnO compacts: effect of temperature on densification and grain growth. *J Am Ceram Soc* 2008;**91**:56–63.

32. Wang XH, Chen IW. Sintering of nanoceramics. In: Gogotsi Y, editor. *Nanomaterials handbook*. New York: CRC Press; 2006. p. 361–83.

33. Wang CJ, Huang CY, Wu YC. Two step sintering of fine alumina–zirconia ceramics. *Ceram Int* 2009;**35**:1467–72.

34. Hesabi ZR, Haghighatzadeh M, Mazaheri M, Galusek D, Sadrnezhaad SK. Suppression of grain growth in sub-micrometer alumina via two-step sintering method. *J Eur Ceram Soc* 2009;**29**:1371–7.

35. Li J, Gong HY, Shi RX, Yin YS. Rising crack–growth–resistance behavior of Al_2O_3 based composites toughened with Fe_3Al intermetallic. *Ceram Int* 2007;**33**:811–4.

36. Qiao ZH, Ma XF, Zhao W, Tang HG, Zhao B. Nanostructured novel cemented hard alloy obtained by mechanical alloying and hot-pressing sintering and its applications. *J Alloy Compd* 2008;**462**:416–20.